Synthesis and Electronic Phosphorescence of Dicyanooctatetrayne (NCN) in Cryogenic Matrixes

Urszula Szczepaniak, Robert Kolos, Marcin Gronowski, Michèle Chevalier, Jean-Claude Guillemin, Claudine Crépin

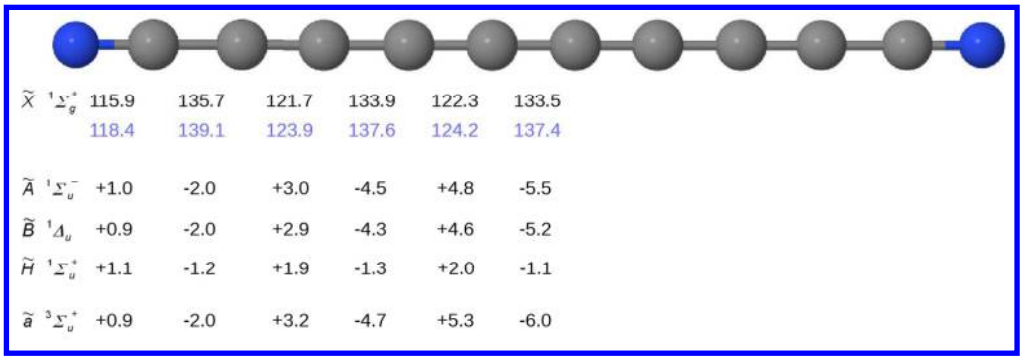

NC10N geometry in its ground and selected excited electronic states...

495x166mm (96 x 96 DPI)

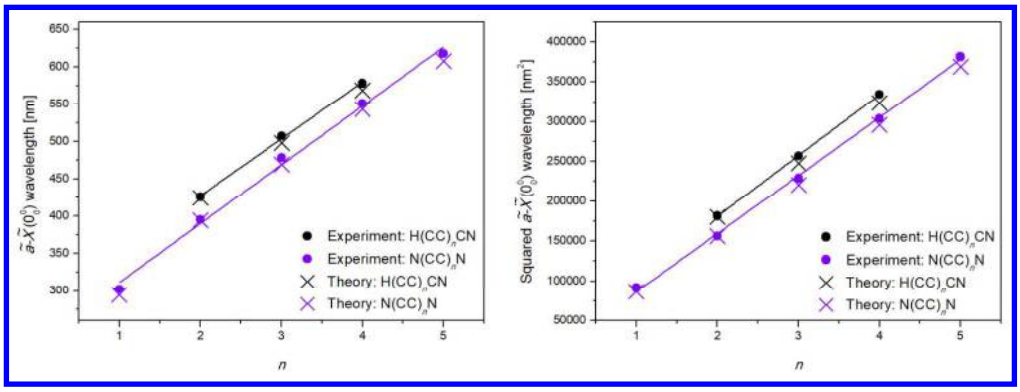

The dependence of phosphorescence wavelength...

468x171mm (96 x 96 DPI)

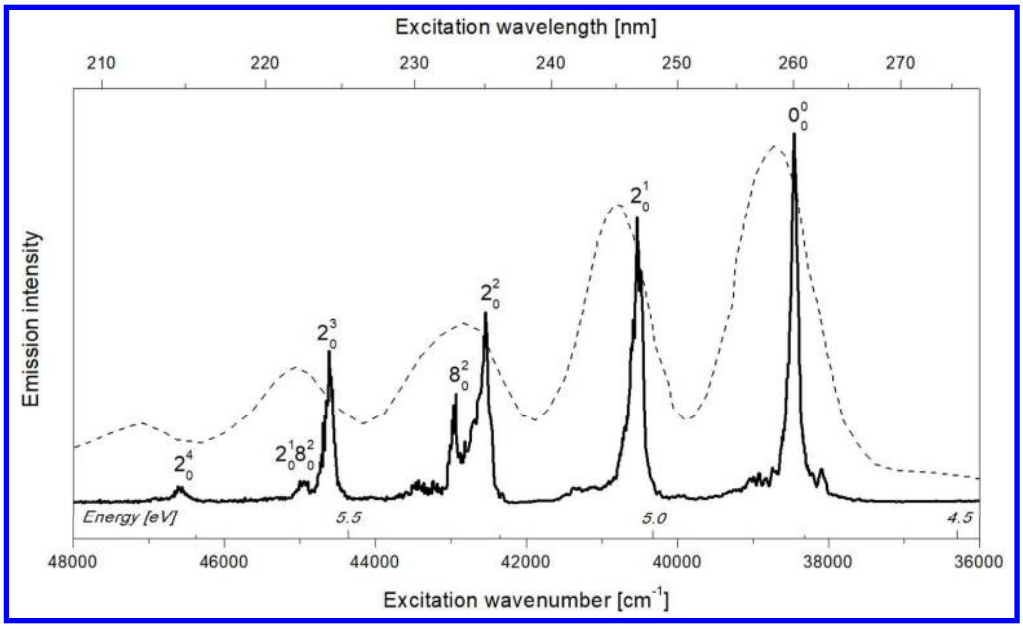

Excitation spectrum of NC10N phosphorescence...

400x242mm (96 x 96 DPI)

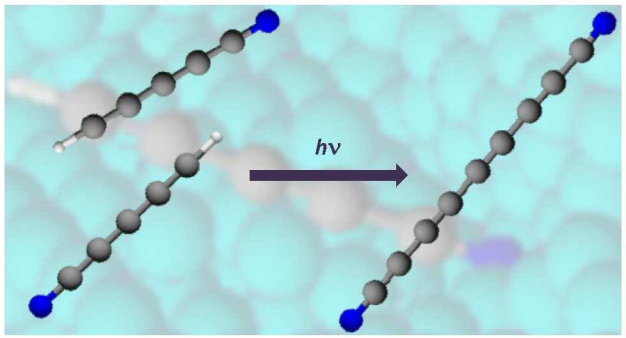
hν

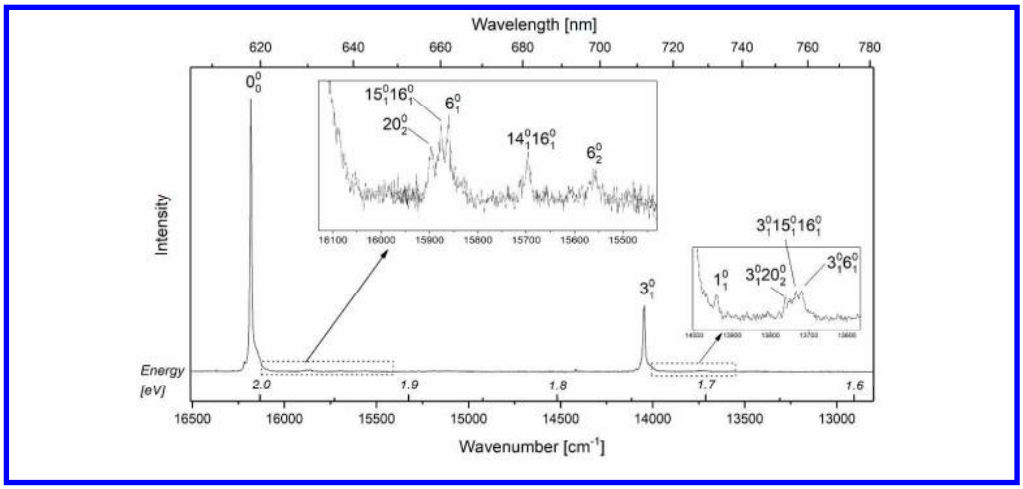

Luminescence, assigned to NC10N phosphorescence, from a previously photolysed (193 nm) Kr/HC5N (1000/1) matrix, excited at 38 390 cm-1 (4.76 eV, 260.5 nm).

431x201mm (300 x 300 DPI)

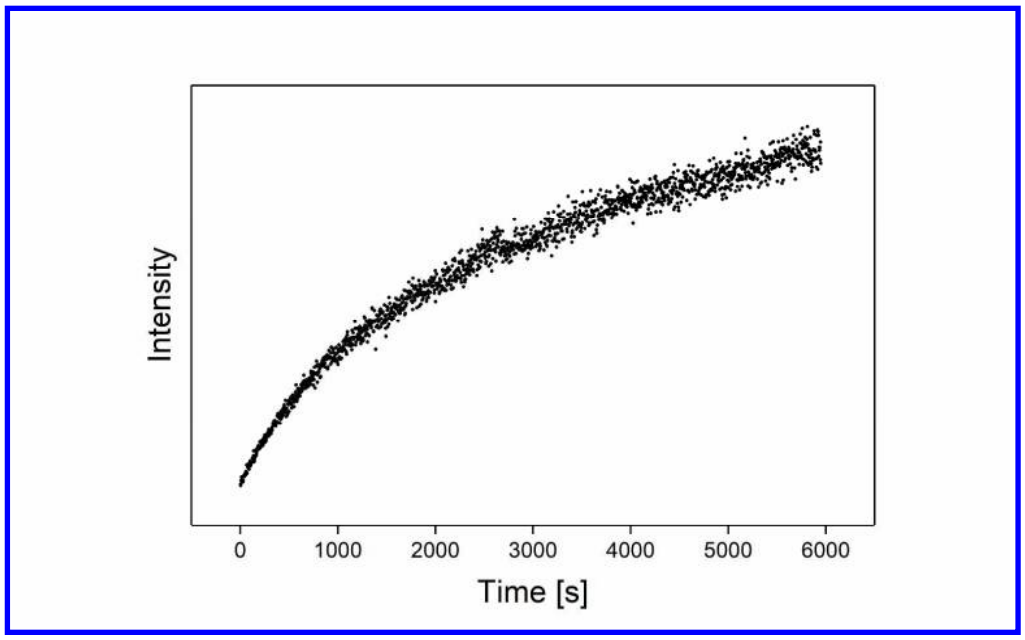

Time evolution of NC10N formation, as monitored by intensity of phosphorescence emitted from irradiated (193 nm) Kr-isolated HC5N. The abscissa represents the irradiation time.

330x203mm (300 x 300 DPI)

Synthesis and Electronic Phosphorescence of Dicyanooctatetrayne ($NC_{10}N$) in Cryogenic Matrices

Urszula Szczepaniak,[a, b] * Robert Kołos,[b] Marcin Gronowski,[b] Michèle Chevalier,[a] Jean-Claude Guillemin,[c] and Claudine Crépin[a]

[a] *Institut des Sciences Moléculaires d'Orsay (ISMO), UMR8214, CNRS, Univ. Paris-Sud, Université Paris-Saclay, F-91405 Orsay, FRANCE,*
[b] *Institute of Physical Chemistry, Polish Academy of Sciences, Kasprzaka 44/52, 01-224 Warsaw, POLAND,*
[c] *Univ Rennes, Ecole Nationale Supérieure de Chimie de Rennes, CNRS, ISCR – UMR6226, F-35000 Rennes, France*

* *urszula.szczepaniak@u-psud.fr, uszczepaniak@ichf.edu.pl;* Present address: Laboratory of Physical Chemistry, ETH Zürich, Vladimir-Prelog Weg 2, CH-8093 Zürich, Switzerland.

ABSTRACT

Rod-like 1,8-dicyano-octa-1,3,5,7-tetrayne ($NC_{10}N$) molecule was synthesized by UV-assisted coupling of rare-gas matrix-isolated cyanobutadiyne (HC_5N) molecules. Detection of $NC_{10}N$ molecule was possible due to its strong orange-red (origin at 618 nm) electronic luminescence. Excitation spectra of this emission ($\tilde{a}\ ^3\Sigma_u^+ - \tilde{X}\ ^1\Sigma_g^+$ phosphorescence) gave access to studying the fully allowed $\tilde{H}\ ^1\Sigma_u^+ - \tilde{X}\ ^1\Sigma_g^+$ UV system of $NC_{10}N$. The identification of observed spectral features was assisted with quantum chemical calculations. Certain regularities shaping the electronic spectroscopy of $NC_{2n}N$ molecules have been discussed.

INTRODUCTION

Hydrogenless centrosymmetric dicyanopolyyne chains ($NC_{2n}N$) constitute a unique series of well-defined linear molecules of closed-shell electronic structure. They are kinetically more stable, at least as judged by the first elements of the series, than respective isoelectronic species of the related monocyanopolyyne ($HC_{2n+1}N$) or polyyne ($HC_{2n}H$) series.[1] For example, while working with dicyanoethyne (NC_4N)[2] we could observe that it is much less susceptible to decomposition (by polymerization) than cyanobutadiyne (HC_5N)[3] or hexatriyne (HC_6H).[4] Rod-like $NC_{2n}N$ chains, with their highly conjugated bonding and the ensuing semiconductive properties, are interesting from purely theoretical/spectroscopic point of view, but potential applications, as nanowires,[5] were also hypothesized. Moreover, dicyanopolyynes are molecules of astrochemical interest.[6] However, while the presence of $HC_{2n+1}N$ nitriles in interstellar gas clouds has been confirmed with microwave spectroscopy up to $n = 4$,[7–16] little is known about centrosymmetric $NC_{2n}N$ molecules in any extraterrestrial sources, apart from a tentative identification[17] of dicyanoacetylene (NC_4N) in the atmosphere of the Saturn's moon Titan. Aerosols build-up from related, highly unsaturated carbon-

nitrogen polymers may contribute to the Titan's characteristic orange haze.[19] Some information about $NC_{2n}N$ molecules in space can be obtained by observation of their protonated forms.[18]

Certain molecular properties were theoretically predicted for $NC_{2n}N$ molecules, including the geometry, vibrational modes, and electronic transition energies; some of these were derived up to $n = 8$.[5,20–22] NC_2N, NC_4N, and (to a lesser extent) NC_6N are rather well experimentally characterized, being available in macroscopic quantities via preparative organic synthesis. In particular, these are known to emit strong phosphorescence under cryogenic isolation conditions.[21,23,24] Experimental data reported for larger ($n > 3$) members of the series are limited to NMR spectroscopy (in $CDCl_3$, $n \leq 9$),[1] IR spectra of solid substances in NaCl ($n \leq 9$),[1] electronic absorption spectra in liquid organic solvents[1,25–27] ($n \leq 9$) and in the gas phase ($n = 8$),[5] and low temperature electronic phosphorescence ($n = 4$).[21,22,24] Very recently, traces of a long-lived luminescence attributable to $NC_{10}N$ were observed by us in a study primarily devoted to HC_9N spectroscopy.[28] In each of these cases, electronic emission was characterized by at least one prominent vibronic progression with a spacing of 2000 – 2300 cm^{-1}, typical of CC or CN triple-bond stretching modes. Luminescence was also observed for $C_4N_2^+$, $C_6N_2^+$, and $C_8N_2^+$ in cryogenic Ne matrices.[29,30]

Here we report on synthesizing $NC_{10}N$ (1,8-dicyano-octa-1,3,5,7-tetrayne or deca-2,4,6,8-tetrayne-1,8-dinitrile) in noble gas (Ar and Kr) matrices, using the method of cryogenic photochemical coupling, already proved useful for C_6N_2,[21] as well as for the monocyanopolyynes HC_5N,[21,31] HC_7N,[32] and HC_9N.[28] Since NC_6N appeared in photolysed matrices doped with HC_3N,[21] $NC_{10}N$ formation from HC_5N was anticipated, even though HC_5N molecules are larger than HC_3N and their movement in a matrix is even more restricted. The spectroscopic identification of products has been supported using density functional theory calculations of electronic and vibrational energy levels.

EXPERIMENTAL METHODS

Experimental details regarding matrix preparation and spectroscopic characterization of the photochemical products are only briefly summarized here, as these were recently described in our reports on HC_9N[28] and CH_3C_7N.[33]

Precursor molecule, HC_5N, was prepared with the method developed by Trolez and Guillemin.[3] It was purified by pumping while kept at T<200K, directly before the experiment. Solid krypton has been shown to permit strong and spectrally well-resolved luminescence of embedded cyanopolyynes.[21,22] Therefore, it was used here (4.0, Messer), along with, more commonly applied in matrix-isolation spectroscopy, argon (6.0, Messer).

HC_5N molecules were mixed with noble gases at a ratio of 1:1000 to 1:500. The mixture was subsequently trapped on a sapphire substrate window held at either 30 K (Kr) or at 22 K (Ar) inside a closed-cycle helium refrigerator equipped with external CaF_2 windows. The typical amount of deposited gas was 6-8 mmol. Composition of the samples was verified with FTIR spectroscopy. The photochemical transformations were induced with UV irradiation of cryogenic matrices (30 K for Kr; 22 K for Ar) by means of an ArF excimer laser (193 nm, 10 Hz, <5mJ/cm^2 per pulse). Spectra

were recorded for a sample kept at 7 K. Of note, the formation of $NC_{10}N$ was also observed in experiments aimed at HC_9N and CH_3C_7N, involving HC_5N co-deposited with, respectively, diacetylene (see Ref. [28]) and methylacetylene (see Ref. [33]). Certain thus far unpublished results coming from these studies are included in the present report.

The identification of photolysis products relied on selectively excited electronic luminescence, by means of an optical parametric oscillator (OPO). Dispersed phosphorescence was searched for in the 380 – 800 nm range with a resolution of approx. 0.04 nm. The observed emission was also registered as a function of the excitation wavelength (192 – 280 nm), yielding phosphorescence excitation spectra. Time synchronization between laser pulses (193 nm excimer laser for photolysis and a tunable OPO for spectroscopy), as well as the acquisition of phosphorescence signals (with a CCD camera) were provided by a home-made triggering device.

COMPUTATIONAL DETAILS

Although certain theoretical studies devoted to $NC_{10}N$ have already been reported,[20] these did not comprise excited electronic states. Here, experiments implicated electronic excitation, respective quantum chemical calculations were therefore performed; for consistency, predictions concerning the ground electronic state have also been included.

Quantum chemical computations were carried out mainly at the density functional theory (DFT)[34] level, with the GAUSSIAN 09 (Rev. B. 01)[35] program package. Time-dependent methodologies[36–38] and the B3PW91 functional of Perdew and Wang[39–42] were applied for singlet excited electronic states. Energetic separations between the ground and the lowest triplet states were derived employing the CAM-B3LYP[43] functional. Computations made use of the aug-cc-pVTZ[44,45] basis set. This approach supplied molecular geometries, harmonic vibrational wavenumbers, and energies of transitions from the ground to excited electronic states. Additionally, IR absorption intensity and Raman activity values were predicted for the ground electronic state (B3PW91/aug-cc-pVTZ). To account for anharmonicity and inherent deficiencies of the involved theoretical approach, vibrational wavenumbers were scaled with the factor of 0.96.[46,47] Linearity of the carbon-nitrogen backbone in excited singlet electronic states was verified by performing CIS/aug-cc-pVDZ[44,45,48] optimizations (starting from a bent structure) and by looking, at both CIS and DFT levels, for the degeneracy of bending modes. Optimized structures were also checked for the absence of imaginary vibrational frequencies. Vertical excitation energies, together with the corresponding oscillator strengths, were additionally derived at the *ab-initio* level CC2[49–52] (cc-pVTZ basis set), using the Dalton2016[53,54] software. Chemcraft[55] program was employed in the preparation of input data and for the visualization of results. However, the CC2 approach applied here can not be regarded as inherently more accurate than DFT, since our CC2 calculations were performed solely within the vertical approximation.

RESULTS AND DISCUSSION

A. Theoretical predictions

Theoretical results concerning the electronic states of $NC_{10}N$ are collected in Table 1 and Figure 1. The first fully allowed electronic excitation of a ground-state molecule is predicted at 4.65 eV (267 nm). We have checked that the energy of the next allowed transition is around 6.2 eV (vertical approximation), and no transition with oscillator strength similar to that characterizing $\widetilde{H} - \widetilde{X}$ is predicted up to around 7 eV. Formerly reported UV-Vis absorption of $NC_{10}N$ in acetonitrile[1] and in *n*-octane solution[25] is energetically close to the currently predicted $\widetilde{H} - \widetilde{X}$ excitation. Electronic structures characterizing states $\tilde{A}$, $\tilde{B}$, $\tilde{a}$, and $\widetilde{H}$ originate mainly in the HOMO-LUMO excitation. $\widetilde{H}$ state features the smallest deviation from the ground state geometry (see Figure 1), just as reported for the analogous ($\tilde{E}$) state of HC_9N.[28] Transitions to the three lowest excited states ($\tilde{A}$, $\tilde{B}$, and $\tilde{a}$) result in mutually similar changes of geometry (in analogy to what was observed for several alike carbon-nitrogen chains [28,33,56]).

Table 1. Theoretical Predictions[a] of Energy (in eV), Wavelength (in nm), and Oscillator Strength (*f*) for Electronic Transitions of $NC_{10}N$ Departing from the $\widetilde{X}\ ^1\Sigma_g^+$ State[b].

		CC2/cc-pVTZ		DFT		
State	Dominant orbital excitation	Vertical transition energy (wavelength)	*f*	Vertical transition energy (wavelength)	f^c	*0-0* transition energy (wavelength)
$\tilde{A}\ ^1\Sigma_u^-$	$3\pi_g \rightarrow 1\pi_u^*$	3.27 (379)	0	2.62 (473)	0	2.18 (569)
$\tilde{B}\ ^1\Delta_u$	$3\pi_g \rightarrow 1\pi_u^*$	3.39 (366)	0	2.71 (458)	0	2.30 (539)
$\tilde{C}\ ^1\Sigma_g^-$	$3\pi_u \rightarrow 1\pi_u^*$	4.64 (267)	0	4.01 (309)	0	3.74 (332)
$\tilde{D}\ ^1\Delta_g$	$3\pi_u \rightarrow 1\pi_u^*$	4.84 (256)	0	4.16 (298)	0	3.90 (318)
$\tilde{E}\ ^1\Sigma_g^-$	$3\pi_g \rightarrow 1\pi_g^*$	5.92 (209)	0	4.81 (258)	0	4.53 (274)
$\tilde{F}\ ^1\Delta_g$	$3\pi_g \rightarrow 1\pi_g^*$	6.01 (206)	0	4.82 (257)	0	4.54 (273)
$\tilde{G}\ ^1\Sigma_g^+$	$3\pi_u \rightarrow 1\pi_u^*$ $3\pi_g \rightarrow 1\pi_g^*$	5.32 (233)	0	4.84 (256)	0	4.56 (272)
$\widetilde{H}\ ^1\Sigma_u^+$	$3\pi_g \rightarrow 1\pi_u^*$	5.30 (234)	6.1	4.80 (258)	5.2	4.65 (267)
$\tilde{a}\ ^3\Sigma_u^+$	$3\pi_g \rightarrow 1\pi_u^*$	2.59 (479)				2.04 (608)

[a] Obtained with DFT (B3PW91/aug-cc-pVTZ for excited singlet states, CAM-B3LYP/aug-cc-pVTZ for $\tilde{a}\ ^3\Sigma_u^+$) and *ab initio* (CC2/cc-pVTZ) methods.

[b] Ground state electronic configuration is [core] $(1\sigma_u)^2\ (1\sigma_g)^2\ (2\sigma_g)^2\ (2\sigma_u)^2\ (3\sigma_g)^2\ (3\sigma_u)^2\ (4\sigma_g)^2\ (4\sigma_u)^2\ (5\sigma_g)^2\ (5\sigma_u)^2\ (6\sigma_g)^2\ (1\pi_u)^4\ (1\pi_g)^4\ (2\pi_u)^4\ (6\sigma_u)^2\ (7\sigma_g)^2\ (2\pi_g)^4\ (3\pi_u)^4\ (3\pi_g)^4\ (1\pi_u^*)^0\ (1\pi_g^*)^0\ (1\sigma_g^*)^0$.

[c] 0 indicates $f < 5 \cdot 10^{-5}$.

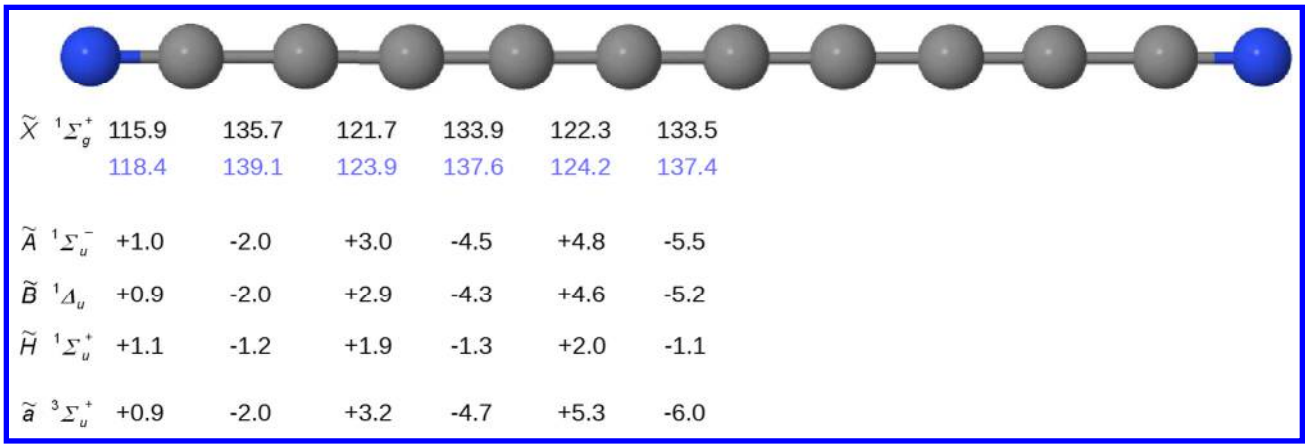

Figure 1. $NC_{10}N$ geometry in its ground and selected excited electronic states as derived at the B3PW91/aug-cc-pVTZ level of theory. Interatomic distances in pm. Values listed for the excited states are relative, calculated with respect to $\widetilde{X}$. Also given (blue) are the RCCSD(T)/aug-cc-pVTZ predictions for the ground state.[20] Geometry predicted for other electronic states listed in Table 1 can be found in Figure S1 of the Supporting Information.

Table 2 lists DFT-derived wavenumbers, IR intensities and Raman activities for the vibrational modes of the ground electronic state, together with respective $\widetilde{H}$-state values (see Table S1 of the Supporting Information for the data concerning other excited electronic states). The visualization of vibrational modes is presented in Table S2 of the Supporting Information.

IR absorption measurements for $NC_{10}N$ dispersed in a solid NaCl film[1] pointed to the spectral features at 2237 cm^{-1} (the strongest one, assigned to CN stretching), 2186, and 2120 cm^{-1}; the first two match well our present prediction of the strongest IR fundamentals (ν_7 and ν_8).

Table 2. Wavenumbers[a] of Vibrational Modes ($\tilde{\nu}$, in cm^{-1}; scaled by 0.96) for $\widetilde{X}\ ^1\Sigma_g^+$ and $\widetilde{H}\ ^1\Sigma_u^+$ Electronic States of $NC_{10}N$. [b] Absolute IR Absorption Intensity (in km/mol) and Raman Scattering Activity (in $Å^4$/amu) Values[a] for $\widetilde{X}\ ^1\Sigma_g^+$ State.

Mode	Symmetry	$\widetilde{X}$			$\widetilde{H}$
		$\tilde{\nu}$	IR intensity	Raman activity	$\tilde{\nu}$
σ symmetry					
ν_1	σ_g	2254	0	7200	2194
ν_2	σ_g	2140	0	150	2067
ν_3	σ_g	2115	0	74000	2017
ν_4	σ_g	1414	0	25	1431
ν_5	σ_g	908	0	52	911
ν_6	σ_g	314	0	4.6	315
ν_7	σ_u	2241	280	0	2174
ν_8	σ_u	2199	20	0	2096
ν_9	σ_u	2061	0.015	0	1941
ν_{10}	σ_u	1180	0.016	0	1190
ν_{11}	σ_u	617	1.1	0	621
π symmetry					
ν_{12}	π_g	554	0	146	509
ν_{13}	π_g	512	0	1.8	462
ν_{14}	π_g	437	0	0.55	392
ν_{15}	π_g	222	0	0.61	210

ν_{16}	π_g	75	0	0.091	75
ν_{17}	π_u	561	3.4	0	515
ν_{18}	π_u	492	11	0	455
ν_{19}	π_u	308	7.0	0	288
ν_{20}	π_u	142	11	0	139
ν_{21}	π_u	28	5.2	0	30

[a] Derived with harmonic approximation at the B3PW91/aug-cc-pVTZ level of theory.
[b] See Table S2 of the Supporting Information for the visualization of vibrational modes.

B. Electronic luminescence

A strong vibronic progression beginning around 615 nm, excited close to 260 nm, appeared in luminescence of HC_5N-doped rare gas matrices previously subjected to ArF-laser irradiations (Figure 2). The new emission can be recognized as phosphorescence of $NC_{10}N$, based on (i) location of the strongest band (16 183 cm^{-1} or 2.01 eV in Kr), a straightforward candidate for the vibrationless origin, matching the theoretical prediction for the $\tilde{a}\ ^3\Sigma_u^+ - \tilde{X}\ ^1\Sigma_g^+$ system (2.04 eV, gas phase); (ii) vibronic spacing (~2140 cm^{-1}; characteristic of a triple-bond stretching); (iii) long luminescence decay time (4.4 ms in Kr); (iv) the nature of precursor species (conceivably capable of doubling its heavy-atom backbone length, just as HC_3N molecules were shown to yield NC_6N).[21] Furthermore, the indicated vibrationless origin (618 nm in Kr or 612.6 nm in Ar) fits well to the general trend already observed for shorter $NC_{2n}N$ molecules (see later in the text).

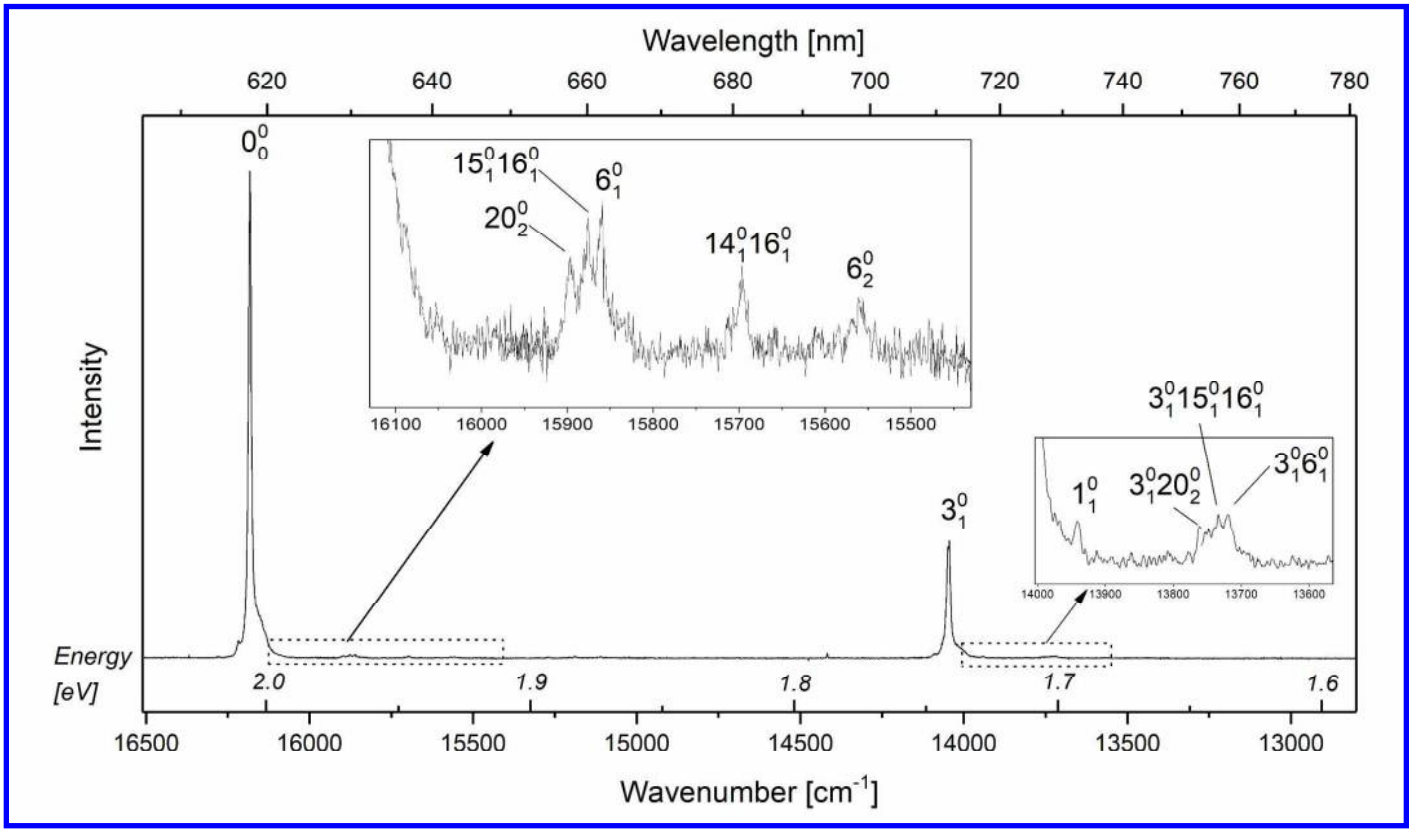

Figure 2. Luminescence, assigned to $NC_{10}N$ phosphorescence, from a previously photolysed (193 nm) Kr/HC_5N (1000/1) matrix, excited at 38 390 cm^{-1} (4.76 eV, 260.5 nm).

The observed main vibronic spacing (see Figure 2) may originate in one of the two *gerade* stretchings, either ν_3 or ν_2, with DFT-predicted wavenumbers of 2115 cm^{-1} and 2140 cm^{-1}, respectively. Although this last value better matches the observed separation of progression elements, the former is preferred, based on its particular molecular distortion pattern: alternate shrinking-expansion of interatomic distances along the chain (see Table S2), qualitatively similar to the geometry change experienced by $NC_{10}N$ upon the transition from $\tilde{X}$ to $\tilde{a}$ (Figure 1). Moreover, the ν_3 stretching is distinct by its highest Raman scattering activity (see Table 2), and such modes were already shown to shape the main vibronic progressions of phosphorescence emitted by shorter $NC_{2n}N$ molecules.[2,21–23,57] Table 3 lists all vibronic bands presently identified in the $\tilde{a}\ ^3\Sigma_u^+ - \tilde{X}\ ^1\Sigma_g^+$ system of $NC_{10}N$. The appearance of only one strong progression governed by a single mode (C≡C stretching), with very few other vibrations contributing to the recognized weak bands, is consistent with the linearity of the lowest triplet state, predicted by DFT calculations. One can notice that in the phosphorescence of $NC_{2n}N$ molecules, relative intensity of bands that do not involve the specific C≡C stretching (analogous to ν_3 here) diminishes with *n* growing from 2 to 5.[2,57]

Weak phosphorescence bands appearing in Kr matrices, blue-shifted from the main spectral features, can be clearly assigned, to a minor matrix site (origin at 16220 cm^{-1}), based on phosphorescence excitation spectra (see below). In Ar-matrix spectra (the Kr-Ar matrix shift is quite large, see Table 3), only the strongest bands have been identified.

Table 3. Vibronic Bands in $NC_{10}N$ Phosphorescence. Relative Values Give the Distance from the Vibrationless Origin.

Wavenumber [cm^{-1}]				Assignment
Kr		Ar		
Absolute	Relative	Absolute	Relative	
16183	0	16324	0	0_0^0
15897	286			20_2^0
15880	303			$15_1^0 16_1^0$
15861	322			6_1^0
15699	484			$14_1^0 16_1^0$
15617[a]	566			$6_1^0 20_2^0$
15585[a]	598			$6_1^0 15_1^0 16_1^0$
15562[a]	621			6_2^0
14046	2137	14186	2138	3_1^0
13941	2242			1_1^0
13760	2423			$3_1^0 20_2^0$
13740	2443			$3_1^0 15_1^0 16_1^0$
13720	2463			$3_1^0 6_1^0$

[a] Weak band, observed with wide-open monochromator slits.

Table 4 collects the results of phosphorescence lifetime measurements for solid Kr-isolated mono- and dicyanopolyynes. Within each of these families, emission lifetime markedly decreases with the increase of polyyne length, a trend that may be explained considering the associated enhancement of two factors promoting non-radiative $T_1 \rightarrow S_0$ relaxation channels: reduction of the singlet-triplet gap and the increasing number of vibrational degrees of freedom (leading to high density of states). Monocyanopolyynes of Table 4 are characterized by faster phosphorescence decays than the respective (*i.e.* isoelectronic) dicyanopolyynes, which may again be due to the higher number of vibrational modes of the former. Moreover, one may point to a possible special role of large CH stretching quanta in coupling T_1 with the ground electronic state.

Table 4. Phosphorescence Decay Time (in ms) for Mono- and Dicyanopolyynes Isolated in Solid Kr.

HC_nN	τ	NC_nN	τ
HC_5N [a]	40	NC_4N [b]	52
HC_7N [c]	8	NC_6N [d]	35
HC_9N [e]	3.9	NC_8N [d]	13
		$NC_{10}N$ [f]	4.4

[a] From Ref. [58]. [b] From Ref. [2]. [c] From Ref. [33]. [d] From Ref. [57]. [e] From Ref. [28]. [f] This work.

A systematic change of electronic transition energy with the molecular size is expected to occur in homologous series (in particular those of unsaturated carbon-chain molecules) for vibrationless transitions sharing a common electronic provenance.[59] Such regularities can be simplistically described either by a particle-in-a-box model (where a 'particle', i.e. an electron, is delocalized in a 'box' formed by a system of conjugated bonds)[60] or by a harmonic oscillator model (with electrons oscillating within π orbitals).[61] It should then be manifested, respectively, by the linear correlation of chain size with either $\lambda_{\mathrm{origin}}$ or $\lambda^2_{\mathrm{origin}}$. Forney et al.[62] reported on linear $\lambda_{\mathrm{origin}}$ vs. n relations for the first allowed electronic absorption systems in several series of highly unsaturated carbon-backbone molecules: $HC_{2n+1}N^+$, $NC_{2n}N^+$, $HC_{2n}N^+$, and $NC_{2n+1}N^+$. The same properties have been found for $C_{2n}H^-$, $C_{2n+1}H^-$, $HC_{2n}H^-$, $HC_{2n+1}H^+$, $HC_{2n+1}H$, C_{2n+1}, and C_{2n+1}^- families.[63] This can be rationalized in terms of a high delocalization of electrons involved in the considered transitions. On the other hand, certain curvature of $\lambda_{\mathrm{origin}}$ vs. n plots, evident for $n > 4$ in the neutral polyyne ($HC_{2n}H$) series, was associated by Pino et al.[63] with more pronounced localization of π orbitals. In such cases, as demonstrated by Hausser et al.[64] for diphenylpolyenes, a $\lambda^2_{\mathrm{origin}}$ vs. n relation (Lewis-Calvin plot) is expected to offer good linearity. Figure 3 presents the $\tilde{a} - \tilde{X}$ vibrationless origin wavelength data for $NC_{2n}N$, and also for the recently analyzed $HC_{2n+1}N$ series. These are neutral, closed-shell structures just as unsubstituted polyynes. Indeed, slightly better linear fits are obtained when $\lambda^2_{\mathrm{origin}}(n)$ rather than $\lambda_{\mathrm{origin}}(n)$ relation is applied. This can be best seen for the largest (5-element) sequence of values collected here, i.e. dicyanopolyynes.

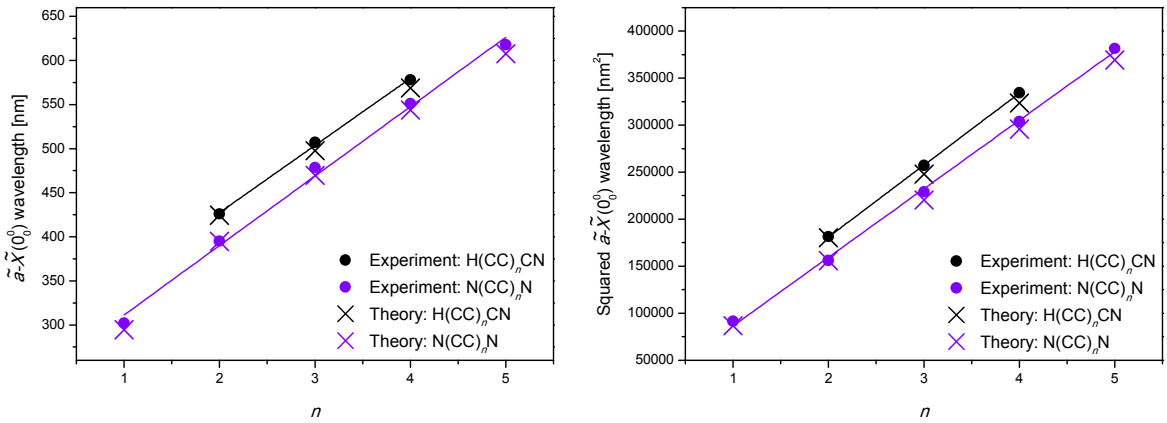

Figure 3. The dependence of phosphorescence wavelength λ_{origin} (left panel) and λ^2_{origin} (right panel) on molecular size, for the series of cyanopolyynic molecules photochemically formed in solid Kr. Experimental values for NC_2N, NC_4N, NC_6N, and NC_8N come from Refs. 2,21–23. Theoretical values as derived at CAM-B3LYP/aug-cc-pVTZ level of theory. Experimental values were fitted with linear functions. The R2 values of fits for dicyanopolyynes are 0.999 and 0.995 for the quadratic and linear functions, respectively. Respective values for monocyanopolyynes are: 0.99997 and 0.99856.

Lines defined by $NC_{2n}N$ and $HC_{2n+1}N$ data (Figure 3) appear to be parallel to each other (with a slope of approx. 75 000 nm^2/triple bond). This can be interpreted as the inclusion of an extra –C≡C– unit having the same effect in both series. It makes yet another similarity between the phosphorescence properties of respective di- and monocyano species. In case of the first fully allowed ($^1\Sigma_u^+ - {}^1\Sigma_g^+$) system observed for $NC_{2n}N$ (n = 3 to 8) solutions in acetonitrile (Ref. [1]), the slope of a Lewis-Calvin plot is much lower (~12 000 nm^2/triple bond) than for the presently discussed phosphorescence, reflecting differences in electronic structure of the lowest triplet ($^3\Sigma_u^+$) and the lowest singlet ($^1\Sigma_u^+$) state (evidenced also by their dissimilar geometries; see Figure 1).

C. Singlet excited electronic states

The phosphorescence excitation spectrum of Kr matrix-isolated $NC_{10}N$ is shown in Figure 4. The first intense band falls around 38 500 cm^{-1} (4.77 eV, 260 nm), in good agreement with the predicted vibrationless onset of the fully allowed $\tilde{H}\ ^1\Sigma_u^+ - \tilde{X}\ ^1\Sigma_g^+$ system (4.65 eV). When identifying other vibronic bands, one should only consider the involvement of *g*-symmetry vibrations, *i.e.* those preserving the general $g \leftrightarrow u$ selection rule. The proposed assignments are presented in Table 5. We identify the $\tilde{H}$-state mode responsible for the main progression as ν_2, considering that it distorts the molecule in the same way (all in-phase C≡C stretches; see Table S2 of the Supporting Information) as does the ν_3 mode of state $\tilde{X}$, recognized as the one shaping the vibronic structure of phosphorescence. Also, the calculated wavenumber of $\tilde{H}$-state ν_2 better matches the obtained spectral data than that of ν_3. A weak distinct band observed to the red of the identified $\tilde{H} - \tilde{X}$ origin may be tentatively interpreted as due to a lower-lying electronic state, the excitation of which could gain probability *via* Herzberg–Teller vibronic coupling (analogous effects were already evidenced in

$HC_{2n+1}N$ (n = 3, 4) excitation spectra in the region of the first allowed electronic bands).[28,33] Weak features detected to the blue of the main vibronic bands supposedly come from the coupling with phonons and/or from the combination with low frequency bending modes; no reliable assignments can be proposed.

Comparing Ar and Kr matrices, one can notice large differences (up to ~1000 cm^{-1}) in the position of detected spectral features. Moreover, spectral splittings, observed in solid Kr, coming from dissimilar surroundings of embedded molecules (matrix sites) vary between 20 and 180 cm^{-1} (see Table 5). This evidence points to substantial influence of the microenvironment on electronic transitions of this highly polarizable[20] molecule. The role of environment was also demonstrated by slightly differing band wavenumbers, from one sample to another. Due to all these effects and to the high photon energy in the discussed spectral range, the error of measured wavenumber distances could reach 30 cm^{-1}. Nevertheless, systematic irregularities observed in vibronic spacing reflect the contributions from anharmonic interactions. As expected, Kr-to-Ar matrix shifts are larger for $\tilde{H} - \tilde{X}$ than for $\tilde{a} - \tilde{X}$ transitions. The present Kr-matrix spectrum is compared in Figure 4 with the UV absorption of $NC_{10}N$ in liquid acetonitrile[1] (maxima at 259, 246, 235 and 223 nm). Neglecting the widths of spectral features, and hence the number of resolved details, the two spectra resemble one another. Moreover, just as for cryogenic matrix sample, vibronic spacings observed in liquid acetonitrile are not regular. Another $NC_{10}N$ absorption spectrum was reported[25] for a liquid *n*-octane solution, with strong absorption bands at 283, 268, 253, 243, and 232 nm. However, an *n*-octane-to-acetonitrile shift of approx. -3300 cm^{-1} (283 nm[25] vs. 259 nm[1]) is unrealistic, and the attribution given in Ref. [25] seems to be erroneous. Additionally, a $^1\Sigma_u^+ - {}^1\Sigma_g^+$ origin in the vicinity of 240 nm can be deduced for gas-phase $NC_{10}N$ from the interpolation of experimental data reported in Ref. [5], indicating a gas-to-Kr matrix shift of ca. -3200 cm^{-1}. This large redshift is smaller than that due to the matrix (>4000 cm^{-1}) observed for the origin of allowed NC_6N absorption (205 nm in Kr[57], 188 nm in gas phase[65]).

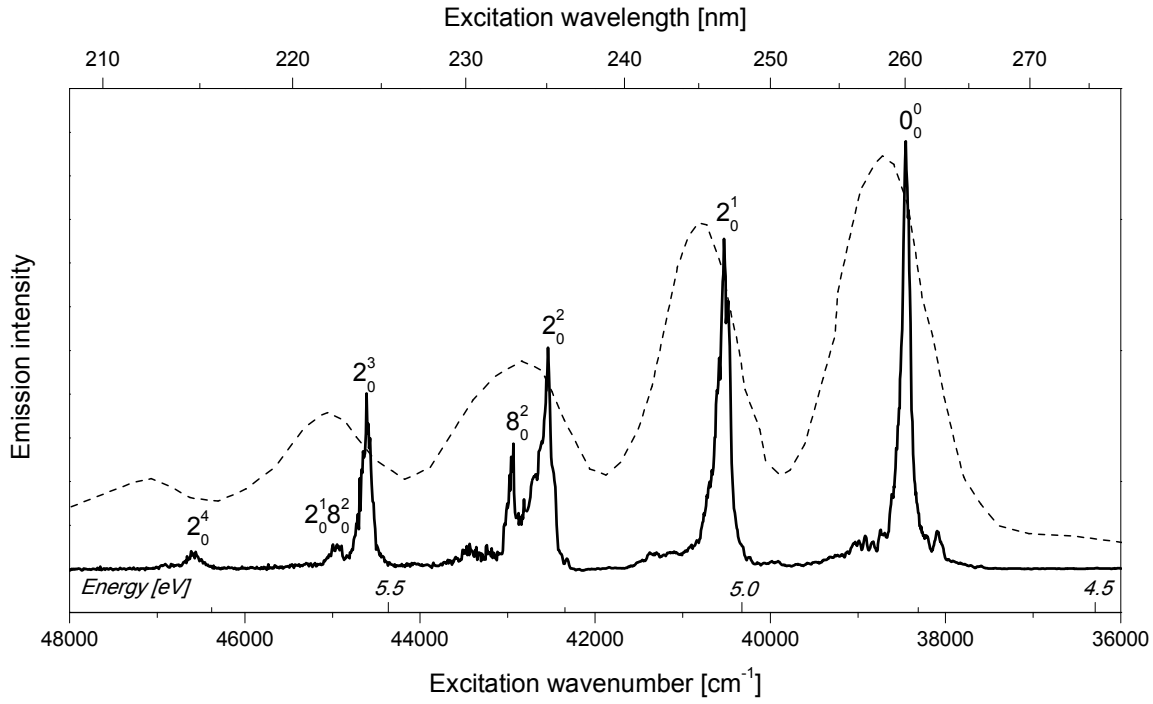

Figure 4. Excitation spectrum of luminescence assigned to $NC_{10}N$ phosphorescence detected at 16 183 cm^{-1} (2.01 eV), as measured for a photolyzed (193 nm) Kr/HC_5N (1000/1) matrix. UV absorption spectrum of $NC_{10}N$ dissolved in liquid acetonitrile (dashed trace; digitized data from Ref. [1]) is given for comparison. Variations of the excitation laser fluence could distort the measured phosphorescence intensity pattern.

Table 5. Vibronic Bands in $NC_{10}N$ Phosphorescence Excitation Spectrum, due to Dipole-Allowed $\widetilde{H}\ ^1\Sigma_u^+ - \widetilde{X}\ ^1\Sigma_g^+$ Transitions. Relative Wavenumber Values Give Distances from the Preceding Progression Elements.

Wavenumber [cm^{-1}]						Assignment
Kr matrix, main site		Kr matrix, minor site		Ar matrix		
Absolute	Relative	Absolute	Relative	Absolute	Relative	
38 470	0	38 610	0	39430	0	0_0^0
40 540	2070	40 700	2090	41440	2010	2_0^1
42 550	2010	42 730	2030	43510	2070	2_0^2
42 950	400	42 970	240			8_0^2
44 600	2050	44 700	1970	45480	1970	2_0^3
44 940	340	45 010	310			$2_0^1 8_0^2$
46 580	1980	46 680	1980			2_0^4
46 910	330					$2_0^2 8_0^2$

D. Formation

Based on previous similar considerations[28,33], one can propose the following $NC_{10}N$ formation scheme:

$$HC_5N + h\nu \rightarrow H^{\bullet} + C_5N^{\bullet}, \quad (1)$$

$$C_5N^{\bullet} + HC_5N \rightarrow NC_{10}N + H^{\bullet}. \quad (2)$$

Radical recombination

$$C_5N^{\bullet} + C_5N^{\bullet} \rightarrow NC_{10}N \quad (3)$$

also has to be considered. This would be analogous to the formation of NC_6N from two $C_3N^{\bullet}$ radicals, elucidated basing on the kinetics of HC_3N photolysis in rare gas matrices.[21] Reaction 3 is however not expected to be of chief importance here, considering the shape of the curve of growth obtained for the $NC_{10}N$ phosphorescence during the photolysis of HC_5N in solid Kr (Figure 5). If the photolysis of matrix-isolated HC_5N molecules had led to $NC_{10}N$ via the recombination of $C_5N^{\bullet}$ radicals then, assuming the validity of arguments provided in Ref. [21] (reporting on the appearance of NC_6N in irradiated HC_3N), one would have seen the original *increase* of the dinitrile production rate with photolysis time. In the present case, the production rate steadily *decreases* from the very onset of irradiations.

Creation of the discussed long, all-heavy-atom chain species requires substantial mobility of the involved precursor chains, apart from their dehydrogenation. Locally increased mobility of reaction partners may be understood in terms of matrix "melting" resultant from the dissipation of the electronic excitation energy. Other products (including mono- and dicyanopolyynes) were detected in the described experiments, but it was not possible to thoroughly investigate their formation efficiencies in terms of kinetics and relative quantum yields.

It is also possible that the precursors, instead of being dissociated into free radicals, are excited to high electronic energy levels and then undergo reactions analogous to Reaction 2. In experiments described here, it is not possible to differentiate between the two cases.

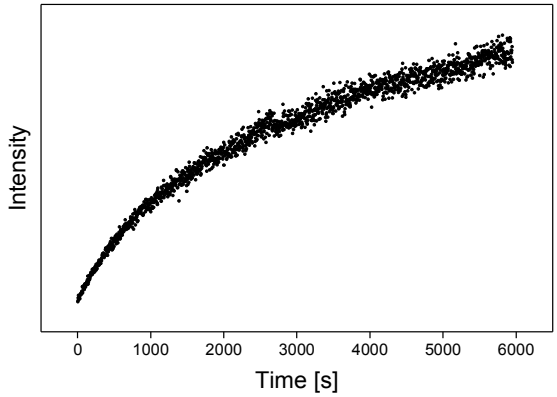

Figure 5. Time evolution of $NC_{10}N$ formation, as monitored by intensity of phosphorescence emitted from irradiated (193 nm) Kr-isolated HC_5N. The abscissa represents the irradiation time.

CONCLUSIONS

The synthesis of a dicyanopolyyne chain as long as $NC_{10}N$ via UV-induced coupling of smaller molecules was observed in Ar and Kr matrices. Strong phosphorescence of $NC_{10}N$ was detected. Vibronic patterns in phosphorescence and phosphorescence excitation spectra were partly interpreted with the assistance of quantum chemical calculations. Among some general trends observed in the series of cryogenic matrix-isolated $NC_{2n}N$ molecules is the lack of fluorescence, which seems to be due to efficient intersystem crossing. Phosphorescence is dominated by a

vibronic progression involving a specific σ_g mode (an in-phase C≡C stretching). With increasing length of the chain:

(i) the wavenumber of that particular mode decreases, approaching the limit defined by the pure collective C≡C stretch of an infinite chain, with vanishing contributions from terminal C≡N groups;

(ii) phosphorescence origin bands become more and more prominent; their wavelengths closely follow a Lewis-Calvin relation (linearity of $\lambda^2_{\mathrm{origin}}$ vs. n);

(iii) energy of the first allowed ($^1\Sigma_u^+ - {}^1\Sigma_g^+$) transition decreases.

Vibronic progressions observed for the $^1\Sigma_u^+ - {}^1\Sigma_g^+$ system are governed by the same specific σ_g stretching that shapes the phosphorescence spectrum. Its energy is lower in the excited state, reflecting a decrease of the C≡C bond strength, compared to the ground state.

Phosphorescence measurement was a detection method of choice in this study aimed at molecule coupling products. The quantity of synthesized $C_{10}N_2$ was too low to produce a detectable IR signature. The reported experimental approach can presumably be adopted to synthesize and study the $NC_{2n}N$ chains of $n > 5$; in particular, present results permit to expect the origin of $NC_{12}N$ phosphorescence in solid Kr at about 670 nm.

ACKNOWLEDGMENTS

This work was financially supported by the Polish National Science Centre, project no. 2011/03/B/ST4/02763, French-Polish scientific cooperation programs *Partenariat Hubert-Curien Polonium* (2012-2013) and *PICS* (2014-2016). U.S. is a beneficiary of the French Government scholarship *Bourse Eiffel*, managed by Campus France, and of the project "Scholarships for PhD students of Podlaskie Voivodeship" – the project is co-financed by European Social Fund, Polish Government and Podlaskie Voivodeship. J.-C.G. acknowledges the financial support received from the Centre National d'Etudes Spatiales (CNES) and from the French program Physique et Chimie du Milieu Interstellaire (PCMI) of CNRS/INSU with INC/INP co-funded by CEA and CNES.

SUPPORTING INFORMATION AVAILABLE

Geometry of $NC_{10}N$ in several electronic states; computed IR wavenumbers for the lowest excited electronic states; visualization of vibrational modes in selected electronic states of $NC_{10}N$. This information is available free of charge via the Internet at http://pubs.acs.org.

REFERENCES

(1) Schermann, G.; Grösser, T.; Hampel, F.; Hirsch, A. Dicyanopolyynes: A Homologuous Series of End-Capped Linear sp Carbon. *Chem. – Eur. J.* **1997**, *3*, 1105–1112.

(2) Turowski, M.; Crépin, C.; Couturier-Tamburelli, I.; Piétri, N.; Kołos, R. Low-Temperature Phosphorescence of Dicyanoacetylene in Rare Gas Solids. *Low Temp. Phys.* **2012**, *38*, 723–726.

(3) Trolez, Y.; Guillemin, J.-C. Synthesis and Characterization of 2,4-Pentadiynenitrile—A Key Compound in Space Science. *Angew. Chem. Int. Ed.* **2005**, *44*, 7224–7226.

(4) Hunsmann, W. Nachweis Und Synthese Des Triacetylens. *Chem. Ber.* **1950**, *83*, 213–217.

(5) Ding, H.; Boguslavskiy, A. E.; Schmidt, T. W.; Maier, J. P. Gas Phase Electronic Spectrum of the Nitrogen Terminated Nanowire $NC_{16}N$. *Chem. Phys. Lett.* **2004**, *392*, 225–228.

(6) Duley, W. W. Chemical Evolution of Carbonaceous Material in Interstellar Clouds. *Astrophys. J.* **2000**, *528*, 841.

(7) Turner, B. E. Detection of Interstellar Cyanoacetylene. *Astrophys. J. Lett.* **1971**, *163*, L35.

(8) Dickinson, D. F. Detection of Cyanoacetylene at 18 GHz. *Astrophys. Lett.* **1972**, *12*, 235–236.

(9) McGee, R. X.; Balister, M.; Newton, L. M. Interstellar Cyanoacetylene J=2→1, J=4→3 Transitions. *Mon. Not. R. Astron. Soc.* **1977**, *180*, 585–592.

(10) Gardner, F. F.; Winnewisser, G. Observations of the J = 1→0 Transitions of the (13) C Isotopic Species of Cyanoacetylene (HCCCN) in the Direction of Sagittarius B2. *Astrophys. J.* **1975**, *197*, L73.

(11) Mauersberger, R.; Henkel, C.; Sage, L. J. Dense Gas in Nearby Galaxies. III - HC_3N as an Extragalactic Density Probe. *Astron. Astrophys.* **1990**, *236*, 63–68.

(12) Bockelée-Morvan, D.; Lis, D. C.; Wink, J. E.; Despois, D.; Crovisier, J.; Bachiller, R.; Benford, D. J.; Biver, N.; Colom, P.; Davies, J. K.; et al. New Molecules Found in Comet C/1995 O1 (Hale-Bopp). Investigating the Link between Cometary and Interstellar Material. *Astron. Astrophys.* **2000**, *353*, 1101–1114.

(13) Snell, R. L.; Schloerb, F. P.; Young, J. S.; Hjalmarson, A.; Friberg, P. Observations of HC_3N, HC_5N, and HC_7N in Molecular Clouds. *Astrophys. J.* **1981**, *244*, 45–53.

(14) Broten, N. W.; Oka, T.; Avery, L. W.; MacLeod, J. M.; Kroto, H. W. The Detection of HC_9N in Interstellar Space. *Astrophys. J.* **1978**, *223*, L105.

(15) Truong-Bach; Graham, D.; Nguyen-Q-Rieu. HC_9N from the Envelopes of IRC+10216 and CRL:2688. *Astron. Astrophys.* **1993**, *277*, 133.

(16) Bell, M. B.; Avery, L. W.; MacLeod, J. M.; Matthews, H. E. The Excitation Temperature of HC_9N in the Circumstellar Envelope of IRC + 10216. *Astrophys. J.* **1992**, *400*, 551–555.

(17) Khanna, R. K.; Perera-Jarmer, M. A.; Ospina, M. J. Vibrational Infrared and Raman Spectra of Dicyanoacetylene. *Spectrochim. Acta Part Mol. Spectrosc.* **1987**, *43*, 421–425.

(18) Agúndez, M.; Cernicharo, J.; Vicente, P. de; Marcelino, N.; Roueff, E.; Fuente, A.; Gerin, M.; Guélin, M.; Albo, C.; Barcia, A.; et al. Probing Non-Polar Interstellar Molecules through Their Protonated Form: Detection of Protonated Cyanogen ($NCCNH^+$). *Astron. Astrophys.* **2015**, *579*, L10.

(19) Waite, J. H.; Young, D. T.; Cravens, T. E.; Coates, A. J.; Crary, F. J.; Magee, B.; Westlake, J. The Process of Tholin Formation in Titan's Upper Atmosphere. *Science* **2007**, *316*, 870–875.

(20) Woon, D. E.; Herbst, E. Quantum Chemical Predictions of the Properties of Known and Postulated Neutral Interstellar Molecules. *Astrophys. J. Suppl. Ser.* **2009**, *185*, 273-288.

(21) Crépin, C.; Turowski, M.; Ceponkus, J.; Douin, S.; Boyé-Péronne, S.; Gronowski, M.; Kołos, R. UV-Induced Growth of Cyanopolyyne Chains in Cryogenic Solids. *Phys. Chem. Chem. Phys. PCCP* **2011**, *13*, 16780–16785.

(22) Turowski, M.; Crépin, C.; Douin, S.; Kołos, R. Formation and Spectroscopy of Dicyanotriacetylene (NC_8N) in Solid Kr. *J. Phys. Chem. A* **2014**, *119*, 2701-2708.

(23) Chang, J.-W.; Lee, Y.-P. The C_2N_2 ã $^3\Sigma_u^+ - \tilde{X}\ ^1\Sigma_g^+$ Chemiluminescence in Matrices. *J. Mol. Struct.* **1987**, *157*, 155–165.

(24) Smith, A. M.; Schallmoser, G.; Thoma, A.; Bondybey, V. E. Infrared Spectral Evidence of N≡C–C≡C–N≡C: Photoisomerization of N≡C–C≡C–C≡N in an Argon Matrix. *J. Chem. Phys.* **1993**, *98*, 1776–1785.

(25) Cataldo, F. Polyynes: A New Class of Carbon Allotropes. About the Formation of Dicyanopolyynes from an Electric Arc between Graphite Electrodes in Liquid Nitrogen. *Polyhedron* **2004**, *23*, 1889–1896.

(26) Cataldo, F. Polyynes and Cyanopolyynes: Their Synthesis with the Carbon Arc Gives the Same Abundances Occurring in Carbon-Rich Stars. *Orig. Life Evol. Biospheres* **2006**, *36*, 467–475.

(27) Forte, G.; D'Urso, L.; Fazio, E.; Patanè, S.; Neri, F.; Puglisi, O.; Compagnini, G. The Effects of Liquid Environments on the Optical Properties of Linear Carbon Chains Prepared by Laser Ablation Generated Plasmas. *Appl. Surf. Sci.* **2013**, *272*, 76–81.

(28) Szczepaniak, U.; Kołos, R.; Gronowski, M.; Chevalier, M.; Guillemin, J.-C.; Turowski, M.; Custer, T.; Crépin, C. Cryogenic Photochemical Synthesis and Electronic Spectroscopy of Cyanotetracetylene. *J. Phys. Chem. A* **2017**, *121*, 7374–7384.

(29) Agreiter, J.; Smith, A. M.; Härtle, M.; Bondybey, V. E. Laser-Induced Fluorescence of Matrix-Isolated $C_4N_2^+$. *Chem. Phys. Lett.* **1994**, *225*, 87–96.

(30) Agreiter, J.; Smith, A. M.; Bondybey, V. E. Laser-Induced Fluorescence of Matrix-Isolated $C_6N_2^+$ and of $C_8N_2^+$. *Chem. Phys. Lett.* **1995**, *241*, 317–327.

(31) Coupeaud, A.; Kołos, R.; Couturier-Tamburelli, I.; Aycard, J. P.; Piétri, N. Photochemical Synthesis of the Cyanodiacetylene HC_5N: A Cryogenic Matrix Experiment. *J. Phys. Chem. A* **2006**, *110*, 2371–2377.

(32) Couturier-Tamburelli, I.; Piétri, N.; Crépin, C.; Turowski, M.; Guillemin, J.-C.; Kołos, R. Synthesis and Spectroscopy of Cyanotriacetylene (HC_7N) in Solid Argon. *J. Chem. Phys.* **2014**, *140*, 044329.

(33) Szczepaniak, U.; Kołos, R.; Gronowski, M.; Guillemin, J.-C.; Crépin, C. Low Temperature Synthesis and Phosphorescence of Methylcyanotriacetylene. *J. Phys. Chem. A* **2018**, *122*, 89–99.

(34) Parr, R. G.; Yang, W. *Density-Functional Theory of Atoms and Molecules*; Oxford University Press, 1989.

(35) Frisch, M. J.; Trucks, G. W.; Schlegel, H. B.; Scuseria, G. E.; Robb, M. A.; Cheeseman, J. R.; Scalmani, G.; Barone, V.; Mennucci, B.; Petersson, G. A.; et al. *Gaussian 09 Rev. B.01*; Gaussian, Inc.: Wallingford, CT, USA, 2009.

(36) Bauernschmitt, R.; Ahlrichs, R. Treatment of Electronic Excitations within the Adiabatic Approximation of Time Dependent Density Functional Theory. *Chem. Phys. Lett.* **1996**, *256*, 454–464.

(37) Casida, M. E.; Jamorski, C.; Casida, K. C.; Salahub, D. R. Molecular Excitation Energies to High-Lying Bound States from Time-Dependent Density-Functional Response Theory: Characterization and Correction of the Time-Dependent Local Density Approximation Ionization Threshold. *J. Chem. Phys.* **1998**, *108*, 4439–4449.

(38) Stratmann, R. E.; Scuseria, G. E.; Frisch, M. J. An Efficient Implementation of Time-Dependent Density-Functional Theory for the Calculation of Excitation Energies of Large Molecules. *J. Chem. Phys.* **1998**, *109*, 8218–8224.

(39) Perdew, J. P.; Ziesche, P.; Eschrig, H. *Electronic Structure of Solids' 91*; Akademie Verlag, Berlin, 1991; Vol. 11.

(40) Perdew, J. P.; Chevary, J. A.; Vosko, S. H.; Jackson, K. A.; Pederson, M. R.; Singh, D. J.; Fiolhais, C. Atoms, Molecules, Solids, and Surfaces: Applications of the Generalized Gradient Approximation for Exchange and Correlation. *Phys. Rev. B* **1992**, *46*, 6671–6687.

(41) Perdew, J. P.; Chevary, J. A.; Vosko, S. H.; Jackson, K. A.; Pederson, M. R.; Singh, D. J.; Fiolhais, C. Erratum: Atoms, Molecules, Solids, and Surfaces: Applications of the Generalized Gradient Approximation for Exchange and Correlation. *Phys. Rev. B* **1993**, *48*, 4978–4978.

(42) Perdew, J. P.; Burke, K.; Wang, Y. Generalized Gradient Approximation for the Exchange-Correlation Hole of a Many-Electron System. *Phys. Rev. B* **1996**, *54*, 16533–16539.

(43) Yanai, T.; Tew, D. P.; Handy, N. C. A New Hybrid Exchange–correlation Functional Using the Coulomb-Attenuating Method (CAM-B3LYP). *Chem. Phys. Lett.* **2004**, *393*, 51–57.

(44) Dunning, T. H. J. Gaussian Basis Sets for Use in Correlated Molecular Calculations. I. The Atoms Boron through Neon and Hydrogen. *J. Chem. Phys.* **1989**, *90*, 1007–1023.

(45) Kendall, R. A.; Jr, T. H. D.; Harrison, R. J. Electron Affinities of the First□row Atoms Revisited. Systematic Basis Sets and Wave Functions. *J. Chem. Phys.* **1992**, *96*, 6796–6806.

(46) Andersson, M. P.; Uvdal, P. New Scale Factors for Harmonic Vibrational Frequencies Using the B3LYP Density Functional Method with the Triple-ζ Basis Set 6-311+G(d,P). *J. Phys. Chem. A* **2005**, *109*, 2937–2941.

(47) Merrick, J. P.; Moran, D.; Radom, L. An Evaluation of Harmonic Vibrational Frequency Scale Factors. *J. Phys. Chem. A* **2007**, *111*, 11683–11700.

(48) Foresman, J. B.; Head-Gordon, M.; Pople, J. A.; Frisch, M. J. Toward a Systematic Molecular Orbital Theory for Excited States. *J. Phys. Chem.* **1992**, *96*, 135–149.

(49) Christiansen, O.; Koch, H.; Jørgensen, P. The Second-Order Approximate Coupled Cluster Singles and Doubles Model CC2. *Chem. Phys. Lett.* **1995**, *243*, 409–418.

(50) Christiansen, O.; Koch, H.; Halkier, A.; Jo/rgensen, P.; Helgaker, T.; Merás, A. S. de. Large□scale Calculations of Excitation Energies in Coupled Cluster Theory: The Singlet Excited States of Benzene. *J. Chem. Phys.* **1996**, *105*, 6921–6939.

(51) Christiansen, O.; Halkier, A.; Koch, H.; Jo/rgensen, P.; Helgaker, T. Integral-Direct Coupled Cluster Calculations of Frequency-Dependent Polarizabilities, Transition Probabilities and Excited-State Properties. *J. Chem. Phys.* **1998**, *108*, 2801–2816.

(52) Hald, K.; Hättig, C.; Jørgensen, P. Triplet Excitation Energies in the Coupled Cluster Singles and Doubles Model Using an Explicit Triplet Spin Coupled Excitation Space. *J. Chem. Phys.* **2000**, *113*, 7765–7772.

(53) Aidas, K.; Angeli, C.; Bak, K. L.; Bakken, V.; Bast, R.; Boman, L.; Christiansen, O.; Cimiraglia, R.; Coriani, S.; Dahle, P.; et al. The Dalton Quantum Chemistry Program System. *Wiley Interdiscip. Rev. Comput. Mol. Sci.* **2014**, *4*, 269–284.

(54) Angeli, C.; Bak, K. L.; Bakken, V.; Christiansen, O.; Cimiraglia, R.; Coriani, S.; Dahle, P.; Dalskov, E. K.; Enevoldsen, T.; Fernandez, B.; et al. *Dalton, a Molecular Electronic Structure Program, Release Dalton2016.2* (2016), see *http://Daltonprogram.org*.

(55) Zhurko, G. *Chemcraft - Graphical program for visualization of quantum chemistry computations* http://chemcraftprog.com/.

(56) Turowski, M.; Szczepaniak, U.; Custer, T.; Gronowski, M.; Kołos, R. Electronic Spectroscopy of Methylcyanodiacetylene (CH_3C_5N). *ChemPhysChem* **2016**, *17*, 4068–4078.

(57) Turowski, M. Niskotemperaturowe Badania Fotochemii i Spektroskopii Cyjanoacetylenów o Znaczeniu Astrofizycznym. PhD Dissertation, Institute of Physical Chemistry, Polish Academy of Sciences, Warsaw, 2012.

(58) Turowski, M.; Crépin, C.; Gronowski, M.; Guillemin, J.-C.; Coupeaud, A.; Couturier-Tamburelli, I.; Piétri, N.; Kołos, R. Electronic Absorption and Phosphorescence of Cyanodiacetylene. *J. Chem. Phys.* **2010**, *133*, 074310–074310.

(59) Murrell, J. N. *The Theory of the Electronic Spectra of Organic Molecules*; Methuen & Co. Ltd: Lomdon, U.K., 1963.

(60) Kuhn, H. A Quantum□Mechanical Theory of Light Absorption of Organic Dyes and Similar Compounds. *J. Chem. Phys.* **1949**, *17*, 1198–1212.

(61) Lewis, G. N.; Calvin, M. The Color of Organic Substances. *Chem. Rev.* **1939**, *25*, 273–328.

(62) Forney, D.; Freivogel, P.; Fulara, J.; Maier, J. P. Electronic Absorption Spectra of Cyano□substituted Polyacetylene Cations in Neon Matrices. *J. Chem. Phys.* **1995**, *102*, 1510–1514.

(63) Pino, T.; Ding, H.; Güthe, F.; Maier, J. P. Electronic Spectra of the Chains $HC_{2n}H$ (n=8–13) in the Gas Phase. *J. Chem. Phys.* **2001**, *114*, 2208–2212.

(64) Hausser, K. W.; Kuhn, R.; Seitz, G. Lichtabsorption Und Doppelbindung. V. Über Die Absorption von Verbindungen Min Konjugierten Kohlenstoffdoppelbindungen Bei Tiefer Temperatur. *Z Phys. Chem Abt B* **1935**, *29*, 391.

(65) Connors, R. E.; Roebber, J. L.; Weiss, K. Vacuum Ultraviolet Spectroscopy of Cyanogen and Cyanoacetylenes. *J. Chem. Phys.* **1974**, *60*, 5011–5024.

TOC Graphic